J Mater Sci (2008) 43:3908–3916
DOI 10.1007/s10853-007-2363-6

Improving the resistance to intergranular cracking and corrosion at elevated temperatures by grain-boundary-engineering-type processing

Ulrich Krupp

Received: 6 July 2007 / Accepted: 29 November 2007 / Published online: 6 March 2008

Abstract Failure of structural components operating under high mechanical loading and/or in aggressive environments can often be attributed to intergranular degradation, e.g. by creep, corrosion, fatigue or brittle cracking. The present article is focussed on oxygen-diffusion-controlled grain-boundary attack, for example, of a nickel-based superalloy leading to intercrystalline oxidation or rapid cracking by dynamic embrittlement. Since grain-boundary diffusion depends on the crystallographic orientation relationship between adjacent grains, the grain-boundary-engineering approach was applied to reduce the susceptibility to grain-boundary attack. The relevant mechanisms are discussed in terms of modifying the network of general high-angle and so-called special grain boundaries taking the results of cracking experiments on bicrystals into account.

Introduction: intergranular material degradation at high temperatures

In many cases the grain boundaries are the weakest links in engineering materials. This can be due to an intergranular enrichment of embrittling species during materials processing, as it is the case, e.g. for temper embrittlement of steels [1], or due to severe service conditions leading to grain-boundary separation by corrosion or creep mechanisms. Particular attention should be paid to loading conditions where a high mechanical load is superimposed by corrosive attack. At ambient temperature such conditions lead to stress-corrosion cracking (SCC), at elevated temperatures the respective damage mechanism has been termed stress-accelerated grain-boundary oxidation (SAGBO, cf. [2]) or dynamic embrittlement (DE, cf. [3, 4]). High-temperature components made of high-strength polycrystalline Ni-base superalloys, e.g. gas-turbine discs of aero engines (see Fig. 1a), may exhibit a superimposition of low-cycle-fatigue (LCF, engine starts/stops) with dwell times during the flights at high tensile load and temperatures of T = 650 °C and above. It has been shown in numerous studies that dwell times or lowering the cycle period during LCF of Ni-based superalloys gives rise to a transition from transgranular to intergranular fracture in combination with a substantial increase in the fatigue-crack propagation rate. Mostly, this phenomenon is attributed to creep-fatigue interactions or oxidation effects. However, at very high-stress amplitudes dwell times may cause quasi-brittle intergranular cracking by dynamic embrittlement [4, 5] that apparently does not involve creep or the formation of thermally grown oxide scales (TGO). Figure 1b and c shows fracture surfaces of the Ni-based superalloy IN718 after LCF loading at 650 °C in air with and without dwell times at maximum tension (σ_{max} = 1,000 MPa). It is worth mentioning that the transition to deformationless intergranular cracking in combination with the dramatic reduction in service life by a factor of seven was not observed when carrying out the same experiment under vacuum conditions, cf. [5].

At temperatures above 800 °C high-temperature corrosion becomes the service-life-limiting degradation mechanism. Since kinetics are diffusion-controlled, the grain boundaries and their structure are key issues in determining the severity of intergranular corrosion attack (cf. Fig. 2a). Only when the temperature exceeds about

U. Krupp (✉)
Faculty of Engineering and Computer Sciences,
University of Applied Sciences Osnabrück, Albrechtstraße 30,
49076 Osnabruck, Germany
e-mail: u.krupp@fh-osnabrueck.de

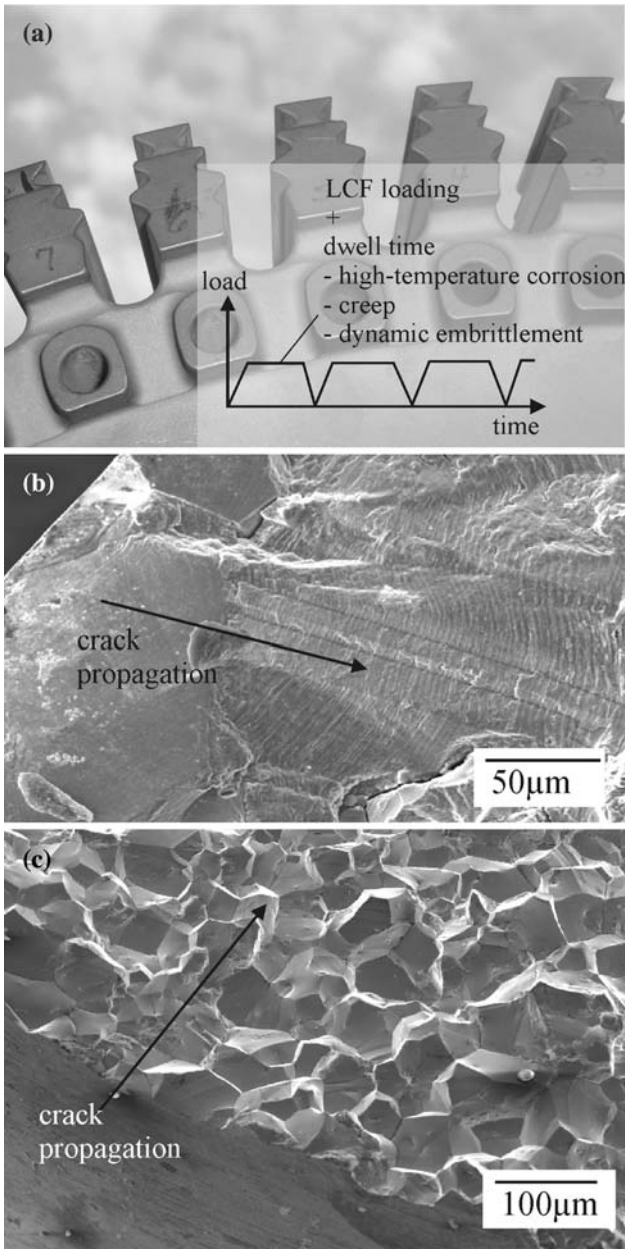

Fig. 1 Dwell-time cracking of nickel-base superalloys: (**a**) gas-turbine disc of alloy 718 and schematic representation of the problem of dwell-time fatigue, (**b**) fracture surface of alloy 718 after fatigue testing at $T = 650$ °C in air ($\Delta\varepsilon/2 = 0.7$) showing typical fatigue striations and (**c**) intergranular fracture surface for a specimen tested under the same conditions than (**b**) with 300 s dwell times at maximum tension

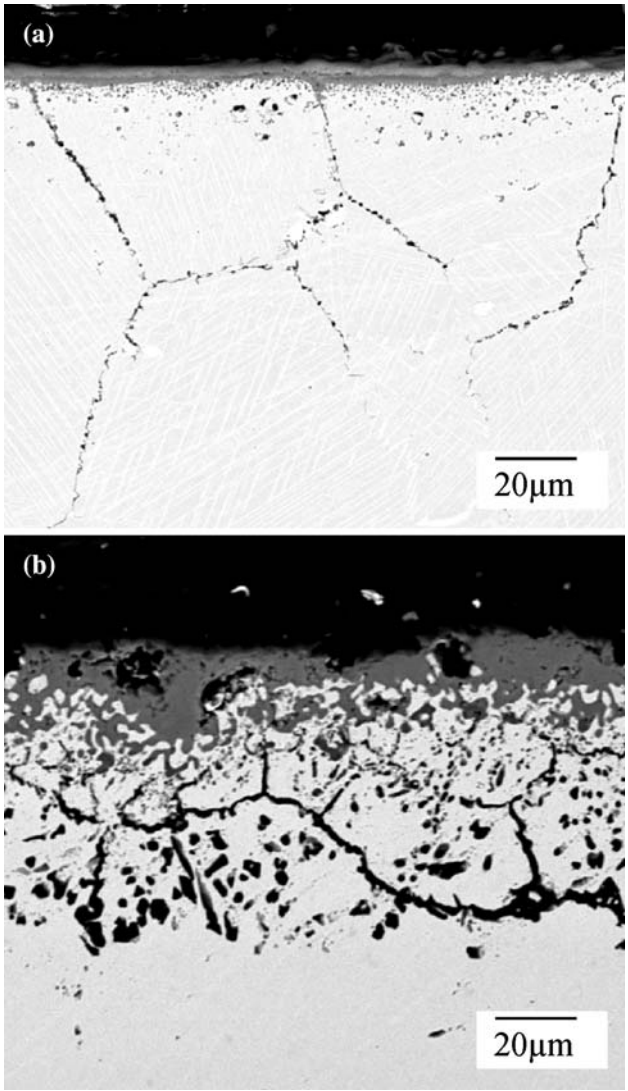

Fig. 2 Cross section of an alloy 718 specimen after 100 h exposure to air, (**a**) at $T = 850$ °C showing strong intergranular Al_2O_3 formation below a superficial Cr_2O_3 scale and (**b**) at $T = 1{,}000$ °C showing homogeneous internal oxidation (Al_2O_3 below Cr_2O_3 scale)

900 °C, bulk-diffusivity becomes sufficiently high to maintain a homogeneous internal-oxidation front. This effect is shown in Fig. 2 for oxidation of alloy 718 in air. At 850 °C the much faster oxygen grain-boundary diffusivity leads to pronounced intergranular Al_2O_3 formation while at 1,000 °C the internal-oxidation depth at the grain boundaries and in the grain interior is roughly the same.

Watanabe was the first who made use of the fact that the grain-boundary properties, such as the GB energy or the GB diffusivity, depend strongly on the GB structures. The great success and development of the automated electron-back-scattered-diffraction technique (EBSD) in the scanning electron microscope (SEM) made fast determination of local crystallographic orientations and evaluation of misorientation-relationship statistics possible (cf. [6]) and hence, Watanabes approach, termed "grain-boundary design" [7], has been systematically shown to increase the resistance to a great variety of intergranular damage mechanisms. "Grain-boundary engineering" (GBE) being the more common designation for the grain-boundary-design approach has been applied, e.g. to SCC and intercrystalline corrosion [8, 9], intercrystalline high-temperature oxidation and cracking

[5, 10, 11], intercrystalline carbide precipitation [12], superplasticity [13], power-law creep [14, 15] or high-cycle fatigue at low and high temperatures [16]. Recently, several recent conference sessions and workshops were devoted to new developments in the field of grain-boundary engineering, the proceedings of them being published as special issues, e.g. [17, 18]. New concepts involve the application of magnetic fields [19] and mechanical stress [20] to achieve an anisotropic improvement of the microstructure or the application of equal-channel angular pressing [21]. Furthermore, more rigorous analyses of the overall geometry and interconnectivity of the grain-boundary planes have been published, e.g. by Randle [22] or Kim et al. [23].

The basic idea of "grain-boundary design" or "grain-boundary engineering" (GBE) is an increase in the fraction of coincident-site-lattice grain boundaries (CSL GBs) with a high fraction of coincident lattice sites between neighbouring grains. Such CSL boundaries should exhibit particular low interfacial energies and "special" properties and be assigned by the respective Σ values, i.e. the reciprocal value of the fraction of coincident lattice sites. For instance, $\Sigma 5$ refers to a grain boundary where every fifth lattice site of the hypothetically interpenetrating crystal lattices of the adjacent grains is coincident, cf. Fig. 3. It should be noted that only in the case of symmetrical tilt boundaries this concept holds true also for the grain-boundary plane itself (cf. [24]). Within an arbitrary grain boundary the number of coincident lattice planes should be generally lower (cf. Fig. 3). However, it should be noted that the spatial positions of grain boundary planes is determined by minimization of the grain-boundary energy being correlated with the crystallographic misorientation.

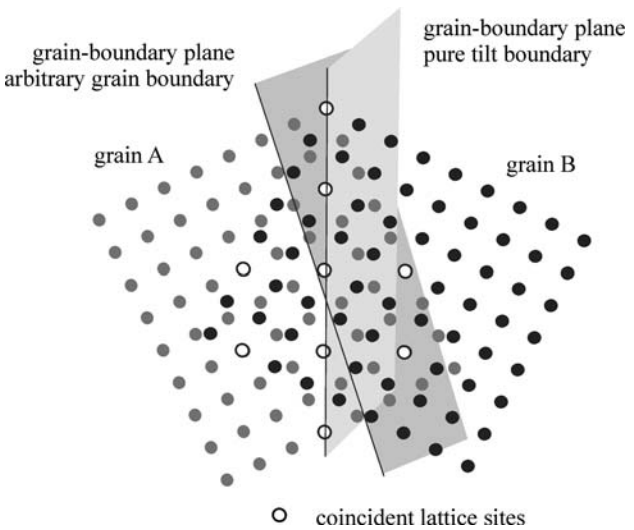

Fig. 3 Schematic representation of two $\Sigma 5$ grain boundaries with a pure tilt and an arbitrary boundary plane

The higher the fraction of special CSL grain boundaries the smaller is the interconnectivity of high-angle general grain boundaries. In the case of intergranular crack propagation an existing crack along a general GB plane should be stopped once it reaches a triple line that meets only special CSL boundaries. According to the Brandon criterion [25] (a more restrictive criterion was suggested by Palumbo and Aust [26])—a boundary is considered to be a CSL boundary when the misorientation falls in an interval $\Delta\Theta$ around the exact CSL misorientation angle,

$$\Delta\Theta = \Delta\Theta_0 \frac{1}{\sqrt{\Sigma}}, \tag{1}$$

with $\Delta\Theta_0 = 15°$ being the limit of a small-angle grain boundary that can be established by geometrically necessary dislocations only.

Grain-boundary-engineering-type processing: experimental details

Materials: GBE-type processing and bicrystal preparation

The material chosen for the intergranular-degradation studies was alloy 718, a polycrystalline Ni-based superalloy that makes up of approximately 40% of all Ni-based alloys used in aero engines. Its chemical composition, the kind of grain-boundary-engineering-type processing (GBE TMP) and the subsequent solution and ageing heat treatment are given in Table 1.

GBE-type processing led to an increase in the fraction of special CSL grain boundaries ($\Sigma 3$–$\Sigma 29$) from a minimum value of $f_{CSL} = 0.149$ in the as-received condition to a maximum value of $f_{CSL} = 0.42$ in the 4-cycle GBE TMP condition, i.e. a thickness reduction by 20% followed by a 1h anneal at 1,050 °C was applied four times. It should be mentioned that approximately 80% of the CSL grain boundaries were $\Sigma 3$ and 4% were $\Sigma 9$.

The maximum strength was obtained by ageing the material resulting in the precipitation of small γ' (Ni_3Al) and γ'' (Ni_3Nb) particles.

The resulting microstructure was characterized by means of scanning electron microscopy (SEM, Philips XL30 LaB_6) in combination with automated electron backscattered diffraction (EBSD TSL orientation imaging microscopy OIM^{TM}). The latter was applied to electropolished specimens to obtain crystallographic orientation mappings which were used to identify special grain boundaries by length fraction according to the CSL scheme.

To get more detailed information about the properties of specific grain boundaries bicrystalline specimens were

Table 1 Chemical composition (in wt.%), heat treatment and GBE-type thermomechanical processing (GBE TMP) of the Ni-base superalloy IN718

Ni	Fe	Cr	Nb	Mo	Ti	Al	Co	Si	Mn	C	B
Bal.	18.7	18.2	5.2	3.0	1.0	0.5	0.1	0.4	0.06	0.04	0.004

Solution heat treatment	1,050 °C (1 h) water-quenched
GBE TMP	Cold-rolling (20%)—annealing 1,050 °C—water quenched (0 (as received) to 4 cycles)
Ageing	720 °C (12 h) furnace-cooled
	620 °C (12 h) air-cooled

prepared by diffusion-bonding. The steps of the preparation process are sketched in Fig. 4 (cf. [27]): Small discs of alloy 718 were cut by spark erosion from single-crystalline rods oriented in such a way that they correspond to the respective orientations to establish the desired bicrystal grain boundary (Fig. 4a). The (310) planes of the discs were put together by rotating them by an angle of 180° to achieve a 37 degree misoriented <100>(310) Σ5 tilt boundary placing them under 10 MPa compression at 1,000 °C in a vacuum furnace (Fig. 4b). Eventually, four-point bending specimens were made from the bicrystals by cutting and adding elongations by vacuum brazing (Fig. 4).

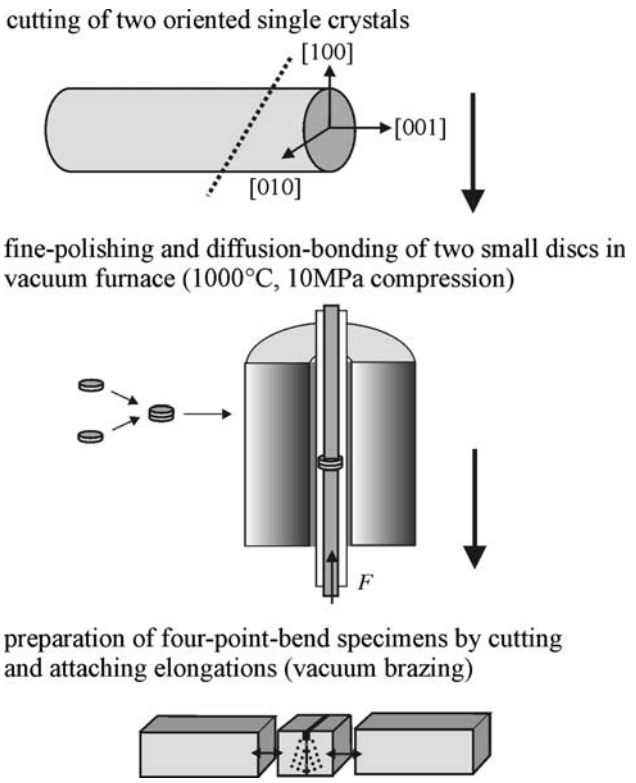

Fig. 4 Schematic representation of the preparation procedure for alloy 718 bicrystals

Testing of mechanical and high-temperature-oxidation behaviour at high temperatures

Fatigue on cylindrical specimens under symmetrical push-pull-loading conditions (cf. [5]) and load-relaxation tests on single-edge-notched bend (SENB) specimens under four-point-bending conditions were carried out at a temperature of $T = 650$ °C in air and under vacuum conditions. Sharp notch tips were produced in the SENB specimens by drawing a thin Mo wire of 100 µm diameter together with 3 µm diamond paste forth and back through the pre-cut side-grooved notch (see Fig. 4). Load-relaxation tests under four-point bending conditions were carried out in a vacuum chamber attached to an electromechanical testing machine. Heating was done by lamps through quartz glass windows. The tests were started by increasing the load up to a certain level and then leaving the cross-head in the respective position. The subsequent load drop corresponds directly to crack advance and was used to calculate the crack velocity (da/dt) versus stress-intensity-factor (K) data (cf. [4, 28]).

High-temperature oxidation kinetics was measured by means of thermogravimetry for exposure at $T = 850$ °C and 1,000 °C to laboratory air. For this purpose small plates were ground by SiC paper (down to 1,200 grit) each of them provided with a small hole and suspended in a thermobalance. The thermobalance consisting of a microbalance of 10 µg resolution, a furnace and a gas-supply system allows to record the corrosion-induced mass gain Δm of the specimen as a function of exposure time t. Such plots represent high-temperature oxidation/corrosion kinetics; in many cases the curves can be described by means of a parabolic rate law in the form

$$\left(\frac{\Delta m}{A}\right)^2 = 2k_p t, \tag{2}$$

with A being the specimen surface and k_p being the parabolic-rate constant, which can be found for single-phase oxidation, e.g. in [29]. Figure 5 shows schematically the experimental setup for four-point-bend testing (Fig. 5a) and thermogravimetry (Fig. 5b).

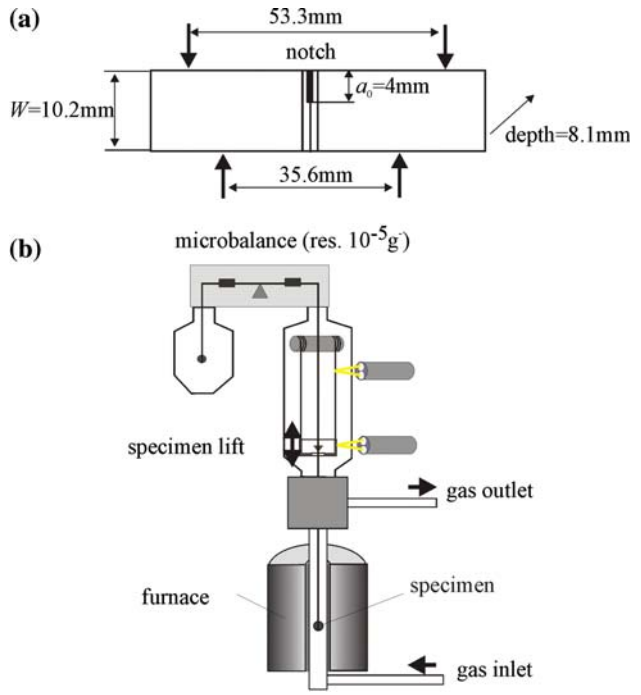

Fig. 5 Schematic representation of (**a**) the geometry and loading points of the four-point-bend specimens and (**b**) the thermobalance to measure the weight change as a function of exposure time

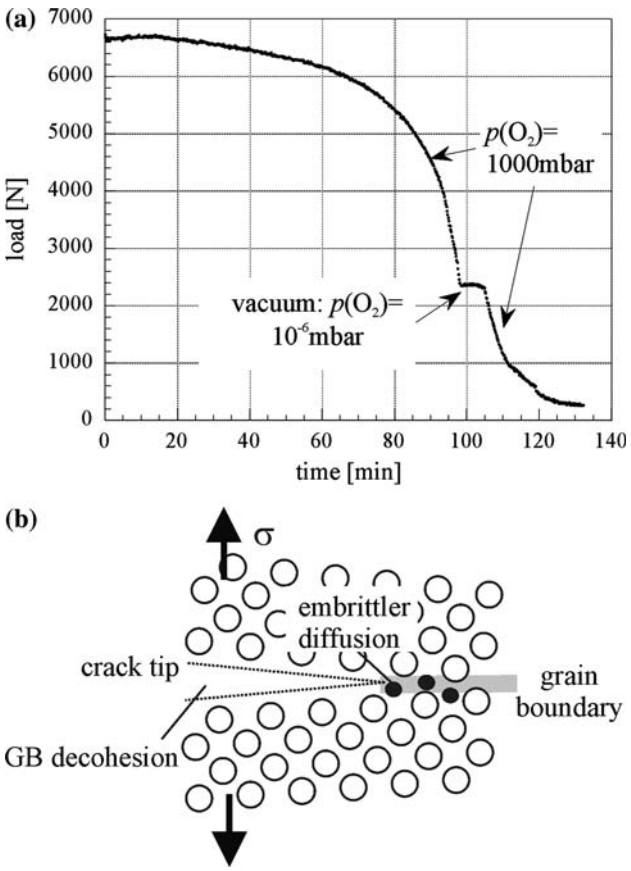

Fig. 6 Intergranular cracking by dynamic embrittlement: (**a**) Load relaxation versus time due to cracking of an alloy 718 specimen at T = 650 °C in oxygen showing complete crack stop when evacuating the testing chamber (Ref. [28]) and (**b**) schematic representation of the dynamic-embrittlement mechanism

Results

The phenomenon of dwell-time cracking during LCF loading (cf. Fig. 1 of the present article) has been studied in detail by static load-relaxation testing under four-point-bend loading conditions. Figure 6 shows a load-relaxation curve of alloy 718 at 650 °C in oxygen taken from the work of Pfaendtner and McMahon [28]. An increase in the slope of the curve corresponds to an increase in the crack-propagation velocity da/dt. When da/dt reached a maximum the testing chamber was evacuated leading to a complete stop of crack propagation. Only when the chamber was backfilled with oxygen again, crack propagation resumed with the same da/dt as before evacuating. The quick response of crack propagation to the availability of oxygen was one of the hints that dwell-time cracking is governed by dynamic-embrittlement, i.e. stress-induced diffusion of elemental oxygen into the grain boundaries lowers the interfacial cohesion and causes quasi-brittle (da/dt $\geq$ 30 μm/s) but time-dependent intergranular fracture (cf. Fig. 6b).

The diffusive flux $\vec{j}$ driven by the gradient in the chemical potential is given as

$$\vec{j} = -\frac{cD}{kT}\nabla\mu. \tag{3}$$

Taking into account that the chemical potential μ of a species is reduced by $\Delta\mu = -\Omega\sigma$, when it is placed inside the substrate material with Ω being its atomic volume:

$$\nabla\mu = -\Omega\nabla\sigma, \tag{4}$$

and the assumed direct relationship between the concentration and the chemical potential, Eq. 3 can be rewritten as

$$\vec{j} = -D\left(\nabla c + \frac{c\Omega\nabla\sigma}{kT}\right). \tag{3}$$

In combination with continuity equation

$$\frac{\mathrm{d}c}{\mathrm{d}t} + \mathrm{div}\vec{j} = 0, \tag{5}$$

and assuming the grain-boundary-diffusion problem to be one-dimensional, the following governing equation for dynamic embrittlement as a combination of Fick's second law of diffusion (first term of the right-hand side of Eq. 6) and a stress term (second term of the right-hand side of Eq. 6) is obtained:

$$\frac{\partial c}{\partial t} = D_{\mathrm{GB}}\frac{\partial^2 c}{\partial x^2} - \frac{D_{\mathrm{GB}}\Omega}{kT}\frac{\partial}{\partial x}\left(c\frac{\partial\sigma}{\partial x}\right), \tag{6}$$

with D_{GB} being the grain-boundary diffusivity (depending on the grain-boundary structure).

It was observed in earlier work by Bika et al. [30] as well as by Krupp [4, 27] that the crack front during crack propagation driven by dynamic embrittlement is not homogeneous. Specimens that were broken open by impact (using a Charpy hammer) after interrupting the dynamic-embrittlement test revealed a great number of unbroken patches left behind the crack front. From these observations the conclusion was drawn that the resistance to dynamic embrittlement depends on the structure and geometrical arrangement of the grain boundaries. It is known from grain-boundary-diffusion studies in metal/metal systems, e.g. [31, 32], that diffusive grain-boundary penetration depends not only on the segregation factor s and the grain-boundary width δ but also on the grain-boundary misorientation angle and structure. For this study it has been assumed that the grain-boundary diffusivity of oxygen is the key driving force for dynamic embrittlement. It is known from the literature that both grain-boundary segregration and grain boundary diffusivity are particularly low for low-angle and special CSL boundaries (cf. [31, 33]). The grain-boundary diffusivity is substantially higher for diffusion parallel to the tilt axis than diffusion perpendicular to the tilt axis (cf. [32]). These assumptions are supported by earlier experiments on Sn-induced dynamic embrittlement of Cu–Sn bicrystals by Muthiah et al. [34] and alloy 718 bicrystals by Krupp [4, 27] and Kane [35]. Four-point-bend tests in air at $T = 650$ °C on bicrystalline specimens of alloy 718 with general high-angle grain boundaries and special Σ5 grain boundaries, with crack propagation parallel and perpendicular to the GB tilt axis as well as crack propagation along a low-angle Σ1 grain boundary revealed (i) a much higher resistance to crack initiation (crack initation at lower K, Fig. 7a) and (ii) much lower crack-propagation velocities for the special CSL boundaries (Fig. 7b). Secondly, the resistance to crack propagation parallel to the GB tilt axis is much lower than the resistance to crack propagation perpendicular to the GB tilt axis [35].

In agreement with the observations made for interfacial crack propagation within different types of grain boundaries in bicrystals, load-relaxation tests under four-point-bend-loading conditions (650 °C, air) on as-received and GBE-type thermomechanically processed specimens of alloy 718 revealed that an increase in the fraction of special CSL grain boundaries leads to a strong decrease in the crack-propagation velocity as well as an increase in the incubation time required for crack initiation. This is shown in the load-drop versus time curves in Fig. 8. As expected, the fracture surface of the GBE-type processed specimen shows a higher fraction (10.5%) of ductile-broken patches

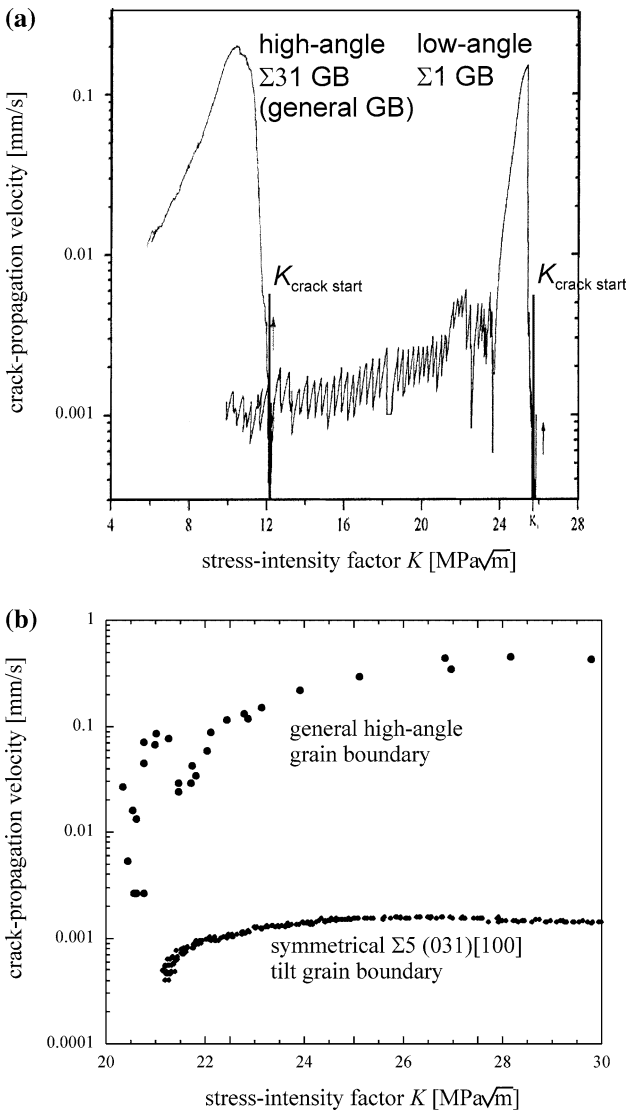

Fig. 7 Crack propagation velocity versus stress intensity factor curves for crack propagation during four-point-bend loading at $T = 650$ °C in air of (**a**) a high-angle Σ31 and a low-angle Σ1 grain boundary [35] and (**b**) a general high-angle grain boundary and a Σ5 grain boundary [4]

than the as-received specimen (5.7%) as revealed by image analysis [36]. The increase by a factor of two can be roughly compared with the respective increase in the fraction of special CSL grain boundaries from the as-received condition (14.9%) to 4-cycle GBE-type processed condition (42.9%).

With the assumption that high-temperature oxidation of alloy 718 in a temperature regime between 700 and 900 °C is at least partly determined by oxygen diffusion being substantially faster along the alloy grain boundaries than through the bulk (cf. Fig. 2), the measured oxidation kinetics in Fig. 9 support the hypothesis that grain-boundary diffusion along special CSL grain boundaries is

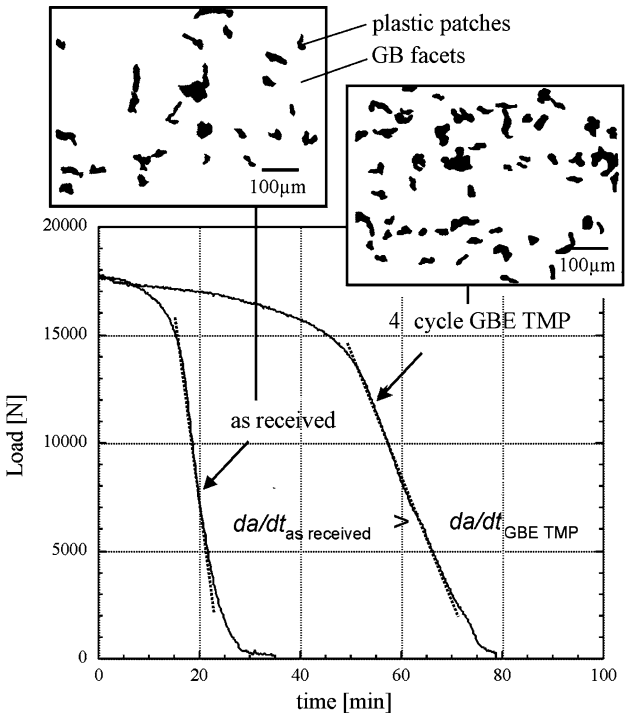

Fig. 8 Load relaxation versus time due to cracking of alloy 718 specimens at T = 650 °C in the as received and the 4-cycle GBE TMP condition, the graphics on top show the quantification of plastically broken patches in the respective fracture surfaces [4, 27]

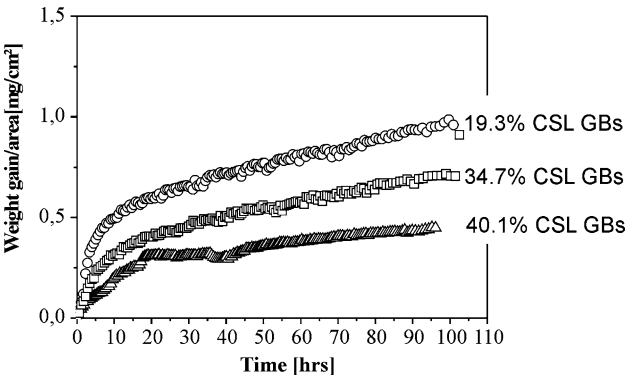

Fig. 9 Thermogravimetarically measured oxidation kinetics (weight gain due to oxidation vs. exposure time) of alloy 718 specimens with different fractions of CSL boundaries exposed at T = 850 °C to air [5]

particularly slow. The higher the fraction of CSL boundaries the lower is the weight gain Δm as a function of exposure time [5].

Discussion

When first dealing with grain-boundary-engineering-type processing it was proposed that increasing the fraction of "special" grain boundaries, i.e. CSL boundaries of $\Sigma \leq 29$ (cf. [37]), gives rise to an increase in the resistance to intergranular attack, which is almost proportional to the CSL boundaries fraction f_{CSL}. This has been shown, e.g. by Lin et al. [9] for intercrystalline corrosion of the Ni-based alloy 600. On the one hand, the thermomechanical procedure to obtain tailored grain-boundary-structure distributions has been systematically improved during the last 10 years; mostly it includes 3–7 times repeated cycles consisting of 20–40% cold work followed by a short-time anneal above the recrystallization temperature [38]. On the other hand, much effort has been put into the analysis of the microstructural changes during grain-boundary-engineering-type processing. Schuh et al. [39] suggested a concept to evaluate the interconnectivity of the general-grain-boundary network. Thus, with an increasing fraction of CSL grain boundaries the general grain boundary network becomes more and more disrupted leaving only short interconnected easy-cracking paths. This is schematically shown in Fig. 10. The grain-boundary-network concept has been further developed and applied to the correlation between macroscopic diffusion and the diffusion along a grain-boundary network of various individual diffusivities [40].

In a more recent article by Yun Bi et al. [41] it was shown that the emission of twins formed as a consequence of thermomechanical treatment leads to a disruption of general GBs (Fig. 11a). Such disruptions give rise to an increased resistance to intergranular corrosion [41] and/or cracking. Figure 11b shows as an example the fracture surface of an alloy 718 four-point-bend specimen that was subjected to load-relaxation at 650 °C in air. While the smooth grain boundary facet is due to quasi-brittle cracking by dynamic embrittlement (see Results section), the twin terminus obviously changed the misorientation relationship in such a way that locally the resistance to brittle cracking was increased. This became obvious by the traces of plastic deformation.

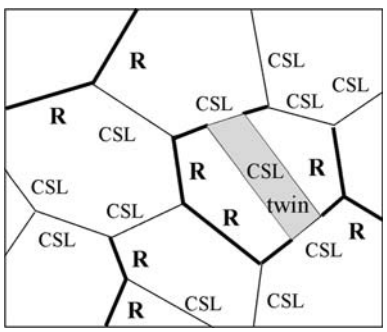

Fig. 10 Schematic representation of disruption of a general grain-boundary network by increasing the fraction of special CSL grain boundaries and twinning

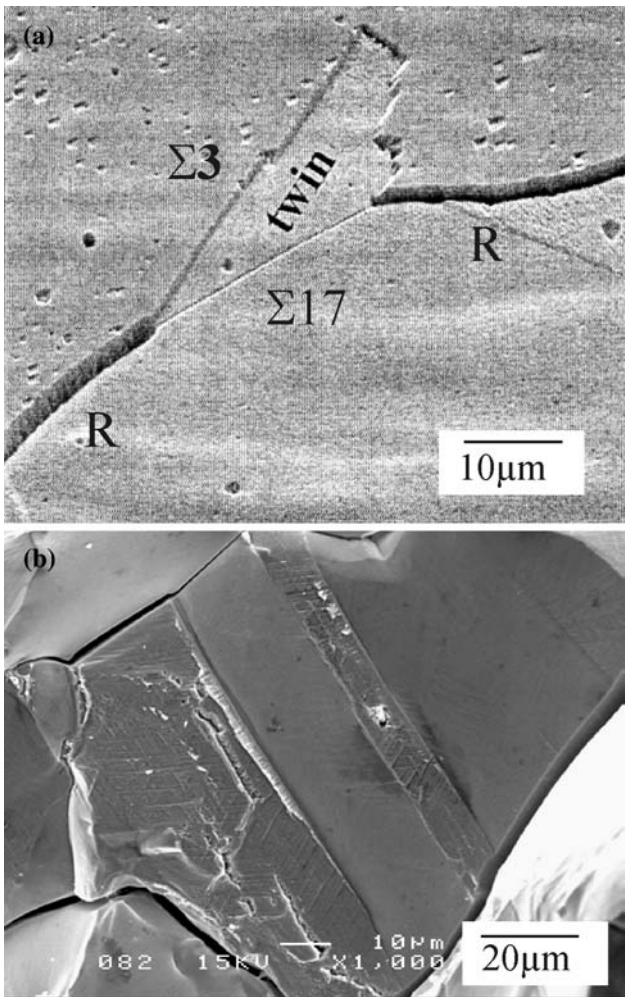

Fig. 11 On the role of twin boundaries for intergranular degradation: (**a**) Twin emission from a general grain boundary leaving a CSL boundary segment that was not attacked by etching (304 stainless steel, [41]) and (**b**) grain-boundary facet with twin terminus in the fracture surface of an alloy 718 four-point-bend specimens after quasi-brittle cracking by dynamic embrittlement at T = 650 °C in air

Modelling of intergranular cracking phenomena governed by grain-boundary diffusion remains challenging. Solutions of the governing equations (cf. Eqs. 3–6) were derived by Xu and Bassani [42] for dynamic embrittlement of Cu–Sn alloys and recently by Klinger and Rabkin [43] for liquid-metal embrittlement (applied to Fe–In and Cu–Bi). However, both approaches are limited to the analysis of bicrystals; discussion of the influence of GBE-type processing on brittle cracking phenomena would require implementation of (i) the resolved normal stress acting on the GB planes (cf. [35]), and (ii) the relationship between the grain-boundary diffusivity and the grain-boundary structure, i.e. misorientation angle, general or CSL GBs, and (iii) the percolation paths of general boundaries exhibiting high diffusivities (cf. [40]). It must also be noted that the increase in the resistance to dynamic embrittlement and high-temperature oxidation cannot solely be attributed to low grain-boundary diffusivity along special grain boundaries. Moreover, a particular low oxygen enrichment can also be expected to be due to the fact that special grain boundaries are regions without segregation (cf. [33]). To answer the question in which way segregation effects superimpose the diffusion effects is subject of ongoing research.

Besides the significance of grain-boundary diffusion on the oxidation kinetics of Ni-base alloys at elevated temperatures the integrity and adhesion of a protective thermally grown oxide scale are important factors determining the material's high-temperature performance. It has been shown by Tan et al. [44] that grain-boundary engineering can alter the microstructure of the oxide scale in such a way that spallation resistance is increased.

Conclusions

Grain-boundary-engineering-type thermomechanical processing (GBE TMP) has been proven to effectively increase the resistance of low-stacking-fault-energy alloys, such as Ni-based alloys or austenitic steels, to intergranular degradation. Among a great variety of damage mechanisms, including power-law creep, fatigue, and stress-corrosion cracking, the GBE TMP approach was applied to two kinds of intercrystalline degradation at high-temperatures that are controlled by oxygen grain-boundary diffusion, intercrystalline oxidation and dynamic embrittlement. It was shown for the Ni-based superalloy 718 that by increasing the number of "special" CSL grain boundaries by a factor of approximately two, the intergranular crack-propagation velocity during four-point bend load-relaxation tests at 650 °C as well as the oxidation rate at 850 °C were substantially decreased. These observations were in agreement with results obtained for bicrystalline specimens of the same material revealing that oxygen diffusion along special CSL boundaries must be by orders of magnitude slower than along general high-angle grain boundaries. Taking structure and mechanical-stress dependence of the grain-boundary diffusion coefficient into account, the efficiency of GBE TMP depends on (i) the frequency of CSL grain boundaries being exposed to high stresses acting normal to the grain-boundary plane and (ii) according to earlier work to the degree of twinning-induced disruption of the general high-angle grain-boundary network.

Acknowledgements The financial support by the U.S. Air Force Office of Scientific Research under grant no. 538532, by the U.S. Department of Energy, Basic Energy Sciences, under grant no. DE-FGO-OIER 45924, the Deutsche Forschungsgemeinschaft (DFG), under grant no. KR1999/7-1 and by the Alexander von Humboldt Foundation through a Feodor Lynen fellowship to the author is

gratefully acknowledged. Furthermore, the author acknowledges the experimental contribution by Dr. William M. Kane, University of Pennsylvania, Philadelphia, USA and Dr. Vicente Braz da Trinade Filho, University of Siegen, Germany, and the many useful discussions with Professor Charles J. MacMahon Jr. and Professor Campbell Laird, both University of Pennsylvania, Philadelphia, USA.

References

1. Pugh SF (1991) An introduction to grain boundary fracture of metals. The Institute of Metals, London
2. Carpenter W, Kang BSJ, Chang KM (1997) In: Loria EA (ed) Proceedings superalloys 718, 625,706 and various derivatives, (TMS 1997). p 679
3. Bika D (1992) Dynamic embrittlement in metallic alloys. PhD thesis, Univ. of Pennsylvania
4. Krupp U (2005) Int Mater Rev 50:83
5. Krupp U, Wagenhuber PE-G, Kane WM, McMahon CJ Jr (2005) Mater Sci Tech 21:1247
6. Randle V (2005) Int Mater Rev 49:1
7. Watanabe T (1984) Res Mech 11:47
8. Shimada M, Kokawa H, Wang ZJ, Sato YS, Karibe I (2002) Acta Mater 50:2331
9. Lin P, Palumbo G, Erb U, Aust KT (1995) Scripta Metall Mater 33:1387
10. Yamaura S, Tsurekawa S, Watanabe T (2003) Mater Trans 44:1494
11. Davé VR, Cola MJ, Kumar M, Schwartz AJ, Hussen GNA (2004) Suppl Weld J 1:1
12. Zhou Y, Aust KT, Erb U, Palumbo G (2001) In: Proceedings processing and fabrication of advanced materials 10 (ASM Intern.). p 438
13. Furuhara T and Maki T (2005) Mater J Sci 40:919
14. Alexandreanu B, Spencer BH, Thaveeprungsriporn V, Was GS (2003) Acta Mater 51:3831
15. Lehockey EM, Palumbo G (1997) Mater Sci Eng A237:168
16. Gao Y, Kumar M, Nalla RK, Ritchie RO (2005) Metall Mater Trans A 36A:3325
17. Watanabe T, Tsurekawa S (eds) (2005) J Mater Sci 40:817
18. Kumar M, Schuh C (eds) (2006) Scripta Mater 54:961
19. Watanabe T, Tsurekawa S, Zhao X, Zuo L (2006) Scripta Mater 54:969
20. Winning M (2006) Scripta Mater 54:987
21. Furukawa M, Horita Z, Langdon TG (2005) J Mater Sci 40:909
22. Randle V (2006) Scripta Mater 54:1005
23. Kim C-S, Rollett AD, Rohrer GS (2006) Scripta Mater 54:1011
24. Randle V (1993) The measurement of grain boundary geometry. Institute of Physics Publ., Bristol
25. Brandon DG (1966) Acta Met 14:1479
26. Palumbo G, Aust KT (1990) Acta Met Mater 11:2343
27. Krupp U (2007) Fatigue crack propagation in metals and alloys. Wiley VCH, Weinheim
28. Pfaendtner JA, McMahon CJ Jr (2001) Acta Mater 49:3369
29. Birks N, Meier GH, Pettit FS (2006) Introduction to the high-temperature oxidation of metals. Cambridge University Press, Cambridge
30. Bika D, Pfaendtner JA, Menyhard M, Mc Mahon CJ Jr (1995) Acta Metall Mater 43:1895
31. Mishin Y, Herzig C (1999) Mater Sci Eng A260:55
32. Kaur I, Gust W (1989) Fundamentals of grain and interphase boundary diffusion. Ziegler-Press, Stuttgart
33. Lejcek P, Hofmann S (1993) Interface Sci 1:163
34. Muthiah RC, Pfaendtner JA, Ishikawa S, McMahon CJ Jr (1999) Acta Mater 47:2797
35. Kane WM (2005) Dynamic embrittlement of nickel-based alloys. PhD thesis, Univ. of Pennsylvania
36. Krupp U, Kane WM, Liu X, Laird C, McMahon CJ Jr (2003) Mater Sci Eng A349:213
37. Palumbo G, Lehockey EM, Lin P (1998) J Mater 2:40
38. Randle V, Owen G (2006) Acta Mater 54:1777
39. Schuh C, Kumar M, King WE (2006) Acta Mater 51:687
40. Chen Y, Schuh C (2006) Acta Mater 54:4709
41. Yun Bi H, Kokawa H, Wang ZJ, Shimada M, Sato YS (2003) Scripta Mater 49:219
42. Xu Y, Bassani JL (1998) Mater Sci Eng A260:48
43. Klinger L, Rabkin E (2007) Acta Mater (in press) (doi: 10.1016/j.actamat.200704.039)
44. Tan L, Sridharan K, Allen TR (2006) J Nuclear Mater 348:263